Seafloor Geodesy

Roland Bürgmann[1] and David Chadwell[2]

[1]Department of Earth and Planetary Science, University of California, Berkeley, California 94720; email: burgmann@seismo.berkeley.edu

[2]Scripps Institution of Oceanography, University of California, San Diego, California 92093; email: cchadwell@ucsd.edu

Annu. Rev. Earth Planet. Sci. 2014. 42:509–34

First published online as a Review in Advance on March 12, 2014

The *Annual Review of Earth and Planetary Sciences* is online at earth.annualreviews.org

This article's doi: 10.1146/annurev-earth-060313-054953

Keywords

crustal deformation, submarine volcanoes, earthquakes, reservoir monitoring

Abstract

Seafloor geodetic techniques allow for measurements of crustal deformation over the ~70% of Earth's surface that is inaccessible to the standard tools of tectonic geodesy. Precise underwater measurement of position, displacement, strain, and gravity poses technical, logistical, and cost challenges. Nonetheless, acoustic ranging; pressure sensors; underwater strain-, tilt- and gravimeters; and repeat multibeam sonar and seismic measurements are able to capture small-scale or regional deformation with approximately centimeter-level precision. Pioneering seafloor geodetic measurements offshore Japan, Cascadia, and Hawaii have substantially contributed to advances in our understanding of the motion and deformation of oceanic tectonic plates, earthquake cycle deformation in subduction zones, and the deformation of submarine volcanoes. Nontectonic deformation related to downslope mass movement and underwater extraction of hydrocarbons or other resources represent other important targets. Recent technological advances promise further improvements in precision as well as the development of smaller, more autonomous, and less costly seafloor geodetic systems.

INTRODUCTION

Geodetic measurements of displacements at Earth's surface have revealed important information about the motion of tectonic plates, the distributed deformation at plate boundary zones, and the dynamics of the earthquake cycle and of active volcanic systems, as well as a range of nontectonic deformation processes. During the past three decades, advances made by using space geodetic systems, such as the global positioning system (GPS) and interferometric synthetic aperture radar (InSAR), have revolutionized our ability to precisely track actively deforming areas with high spatial and temporal resolution (Bürgmann & Thatcher 2013).

Earth is a water planet, with approximately 70% of its surface covered by deep oceans (**Figure 1**). Thus, many important plate boundary zones, volcanoes, and other deforming systems cannot be studied with the established tools of tectonic geodesy, as water is not a suitable medium for geodetic systems that depend on the relatively unperturbed transmission of electromagnetic waves. Seafloor geodesy is aimed at developing tools to study underwater deformation, relying on mechanical or acoustic systems suitable for offshore deployment to measure changes in interstation distances, relative positions, water depth, tilt, or gravity. Over the past three decades, seafloor geodetic techniques have been developed and optimized to achieve measurement capabilities comparable to those obtained on land. Nonetheless, technical challenges and the high cost of seafloor observations have largely limited the application of seafloor geodesy to proof-of-concept studies.

The plate tectonic revolution, and the associated recognition that much of the world's active plate boundaries are hidden under the oceans, provided the rationale for measuring offshore tectonic deformation (Spiess 1985, Spiess et al. 1983). Several tectonic plates, such as the Juan de Fuca, Cocos, Scotia, Nazca, and Philippine Sea plates, have few or no islands on them that

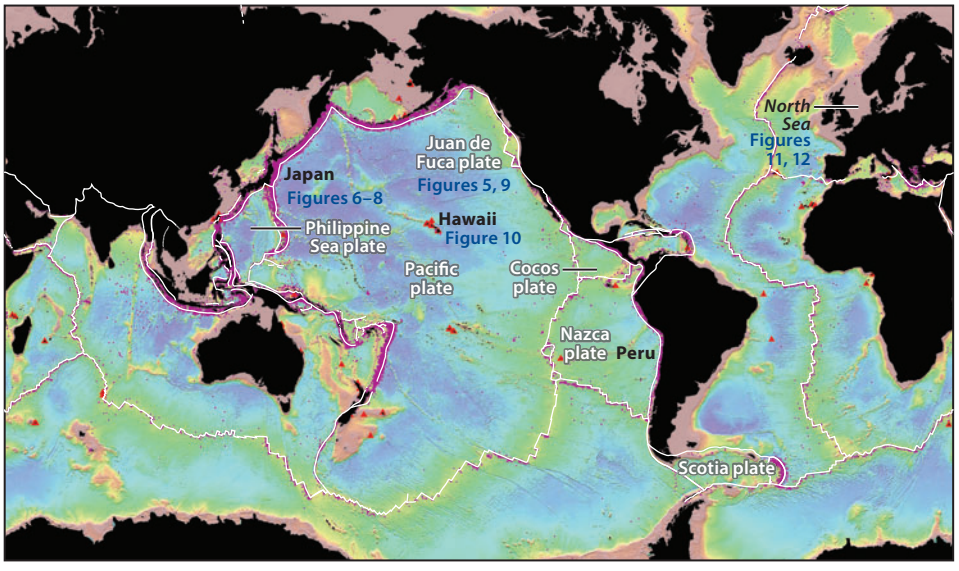

Figure 1

Earth, the water planet. Map of global bathymetry (based on Smith & Sandwell 1997) with submarine tectonic plate boundaries (*white lines*), Holocene volcanoes (*red triangles*), and recent earthquakes from a depth of <70 km (*magenta dots*). Areas targeted with seafloor geodesy and oceanic tectonic plates are labeled.

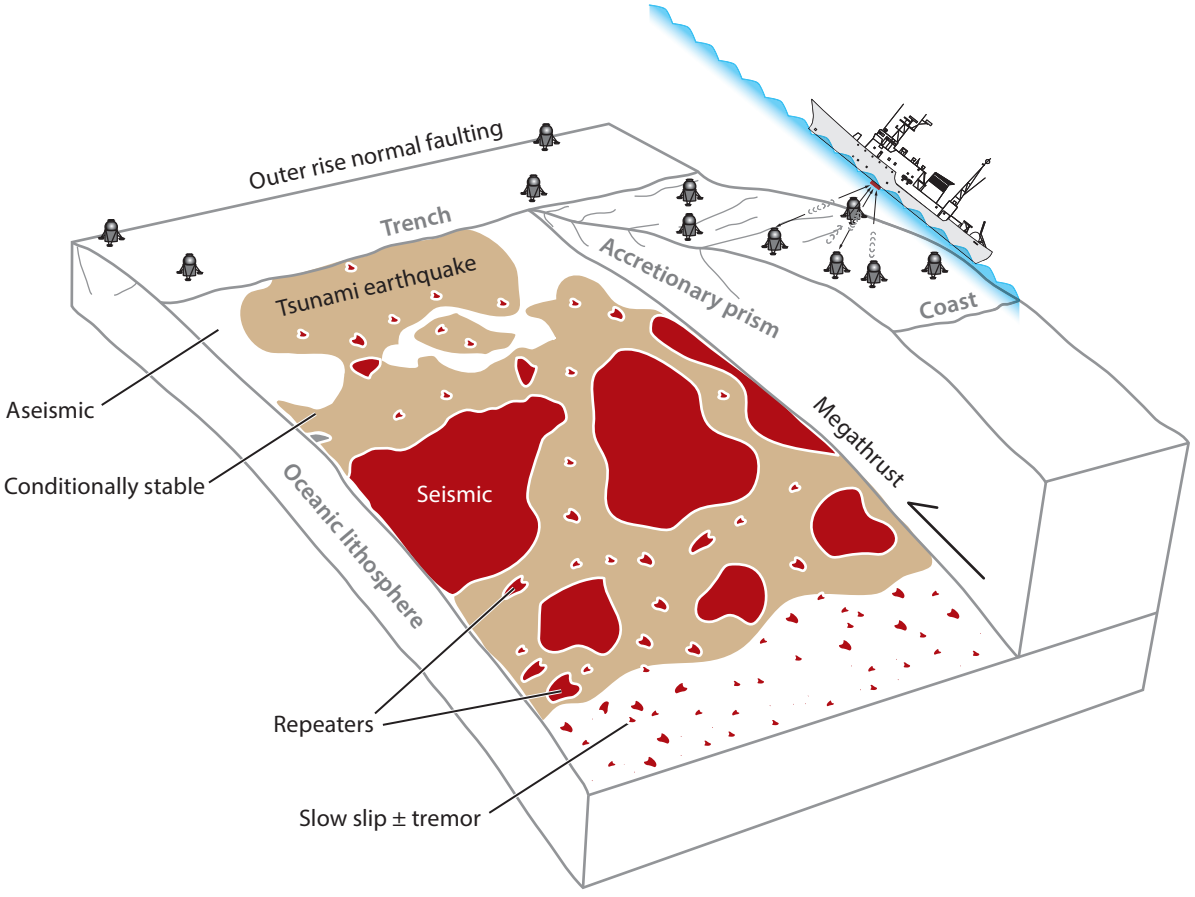

Figure 2

Schematic diagram of subduction zone structure and mechanics (based on Lay et al. 2012). Regions of unstable frictional slip (*red*) represent the rupture zones of large and small earthquakes. Areas of steady or episodic aseismic slip are shown in white. Tan-colored areas are inferred to be conditionally stable and are expected to slip aseismically, except when accelerated to dynamic failure by stress changes from ruptures on adjacent seismic patches.

would allow for easy measurement of their current motion and internal deformation by using space geodetic techniques (**Figure 1**). Most seismic and volcanic activity on Earth occurs underwater. This includes approximately 60,000 km of mid-ocean spreading ridges, where oceanic plates grow by volcano-tectonic processes, and associated transform faults. The most actively deforming portions of the world's subduction zones are covered by water (**Figure 2**). Underwater volcanic activity is also associated with rising mantle plumes that result in the growth of oceanic islands in plate interiors. Such rapidly formed islands tend to be gravitationally unstable and deform by steady, seismic, or catastrophic flank failure. Seafloor deformation is not restricted to active plate boundaries and volcanic systems. Substantial seafloor deformation is also associated with submarine landsliding, hydrocarbon extraction, and CO_2 injection into submarine reservoirs.

Investigators first began to explore seafloor geodetic techniques for vehicle tracking with meter-level precision in the mid-1960s (Spiess et al. 1966). Spiess (1980) proposed that improved

technology, using acoustic transponders and underwater vehicles, and careful consideration of sound velocity variations would enable the deployment of acoustic ranging systems that could track displacements at centimeter-level precision over a few kilometers. Only in the 1980s did improvements to measurement systems provide the capability to track displacements at the precisions needed to capture tectonic deformation (Spiess 1985). The first pressure sensor for measuring vertical deformation was deployed in 1987 on the summit of Axial Seamount, an active volcano along the Juan de Fuca Ridge (Fox 1993). For horizontal positioning, both direct-path systems and integrated GPS-acoustic systems (GPS-A) were developed (Spiess 1980, 1985). Direct-path systems were first installed on the Cleft segment and Axial Seamount on the Juan de Fuca Ridge in the early 1990s (see Chadwell et al. 1999, Chadwick et al. 1999, and references therein). The first seafloor GPS-A station was installed in 1991 to measure the motion of the Juan de Fuca plate near Vancouver Island, Canada (Spiess et al. 1998). Starting in the 1990s, direct-path ranging, GPS-A, and ocean-bottom pressure systems were also developed in Japan and deployed there as well as on the fast-spreading East Pacific Rise (e.g., Fujimoto et al. 1998, Fujita et al. 2006). More recently, the 2011 *M* 9 Tohoku earthquake was a major turning point for seafloor geodesy, showing the importance of such measurements and providing strong motivation for expanding the monitoring network offshore Japan.

Despite the progress that has been made over the past three decades, seafloor geodesy is only slowly beginning to transition from demonstration projects to comprehensive monitoring systems. We expect that the development of more advanced and lower-cost seafloor geodetic systems will lead to more comprehensive monitoring of a wide range of submarine deformation processes and the hazards and resources they reveal. Here, we review the main techniques of seafloor geodesy, summarize key scientific accomplishments enabled by these methods, and close by considering future challenges and opportunities we anticipate for the field.

METHODS OF SEAFLOOR GEODESY

Acoustic Ranging

Acoustic ranging measures distances and their changes with time, through the use of precisely timed sound signals between acoustic transponders on the seafloor or from a vehicle to the transponders. Sound travels at nominally 1,500 m/s through seawater, which requires the time of flight (TOF) to be resolved to within 10 μs for 1.5-cm resolution of distance. A single pulse or cycle of a 100-kHz signal has a wavelength of 1.5 cm, and detecting its arrival is a crude but suitable approach to measure distances from a few tens of meters to 1–2 km. Much beyond this distance the signal is no longer detected, as its strength diminishes rapidly with the square of the path length. To compensate, a signal with a frequency dropped to 10 kHz can easily propagate up to 15 km. The wavelength, however, is now 15 cm, and to maintain a timing resolution of 10 μs, a pulse compression approach must be adopted. The pulse or code is typically from 10 to 20 ms long and consists of frequency steps and/or phase changes. Cross-correlating the original pulse with its return resolves the TOF to a few microseconds.

Extracting geometric distances from the TOF requires accurate knowledge of the medium in which the signal travels, i.e., its motion and sound speed. Currents move seawater at centimeters to decimeters per second, and an acoustic pulse traveling in this medium is likewise advanced or retarded. By measuring the round-trip travel time between two units, the effect over the few milliseconds of an acoustic measurement cycle is practically equal but opposite and cancels. To date, acoustic ranging systems for seafloor geodesy employ round-trip or two-way TOF measurements between an interrogator and a transponder.

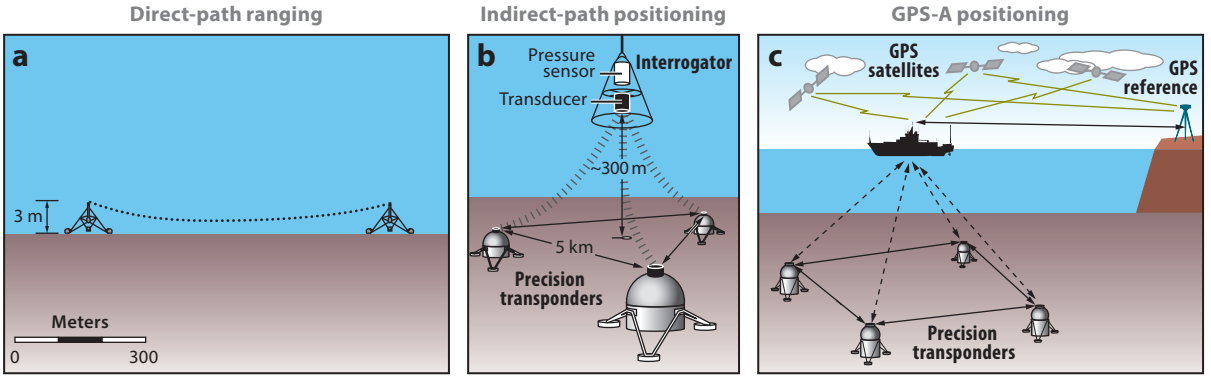

Figure 3

Schematic diagrams of acoustic ranging methods for seafloor deformation measurements (modified from Chadwell & Sweeney 2010). (*a*) Direct-path ranging between two raised transponders. The baseline length is limited by upward refraction of the acoustic signal. (*b*) Indirect-path system using an interrogator to increase range between transponders. (*c*) GPS-A using kinematic GPS positioning of a ship or buoy to precisely determine the location of a transponder array on the seafloor in a global reference frame.

Ultimately, though, the accuracy of underwater acoustic ranging is limited by uncertainty in sound speed. In fact, sound speed dictates three different configurations of acoustic ranging: direct path, indirect path, and surface path to GPS or GPS-A (**Figure 3**). Sound speed in the ocean is controlled primarily by seawater temperature, salinity, and pressure. Surface-driven mixing affects temperature and salinity, which predominantly influence the value of sound speed in the upper ocean. Going deeper, mixing diminishes, temperature and salinity stabilize, and pressure dominates as it monotonically increases with depth. Below a water depth of approximately 1,000 m, acoustic energy is refracted upward due to the sound velocity increase caused by this pressure gradient (**Figure 3*a***). Thus, on a flat seafloor, hydrophones must be raised approximately 3 m to prevent an acoustic signal from hitting the seabed while traveling between points separated by 1 km (e.g., Chadwell et al. 1999, Chadwick et al. 1999). Ray bending increases with the square of the separation, but higher towers are not practical, both from the point of view of deployment and because of the difficulty of isolating tower tilt from baseline change.

To compensate for ray bending, one end of an acoustic range can be floated tens of meters above the seafloor in an indirect-path configuration, and ranges up to a few kilometers can be measured between the interrogator and transponders (**Figure 3*b***). Because the interrogator is no longer rigidly attached to the seafloor, range changes are not direct measures of deformation. The solution is to deploy three or more seafloor transponders and to measure both the depth of the floating interrogator (with pressure sensors) and the ranges to the seabed units. The position of the interrogator has three unknowns and four observations. By collecting ranges from an interrogator moved laterally around the array, or from several individual interrogators/receivers moored throughout the array, the overdetermined information reveals the relative positions of the seafloor units. The indirect-path approach can measure the deformation between seafloor points up to approximately 5 km apart with 1–2-cm resolution (Blum et al. 2010, Sweeney et al. 2005). Multiple direct-path or indirect-path units can be chained together to increase coverage across many kilometers, but they cannot span tectonic plates.

Acoustic ranging alone is not suitable to capture tectonic deformation over tens to thousands of kilometers. Sound speed measurement accuracy is at best approximately 1 to 3 parts in 10^5 of

1,500 m/s or approximately ±0.05 m/s. Ranges based upon the TOF of acoustic signals through the ocean maintain decimeter-level accuracy for at most 10 km. By comparison, the speed of light through Earth's heterogeneous atmosphere is known to approximately 1 part in 10^8, or three orders of magnitude better than the speed of sound in the ocean. Thus, kinematic GPS is used to precisely locate seafloor sites by tracking a sea-surface platform maintained above transponders on the seafloor (**Figure 3*c***). Acoustic ranges from the platform to the transponders connect the GPS positions to the seafloor. This is the essence of the GPS-A approach (Spiess 1985, Spiess et al. 1998).

Whereas sound speed from the surface to the seafloor is predominantly horizontally stratified, sound speed in the upper ocean varies both temporally and spatially over timescales and with magnitudes significant to acoustic ranging. To date, there is no method to measure all these effects independently in situ, but their impact can be mitigated by the design of the acoustic array (Spiess 1985). Three or more transponders are evenly spaced around the perimeter of a circle with a radius of the nominal water depth (**Figure 3*c***). The baselines between the transponders are assumed to be fixed, a reasonable assumption in plate-scale tectonics. These baselines act as yardsticks from which it is possible to measure the time-varying, common-mode sound speed directly from the acoustic ranges pinned at the surface with GPS. Generally, the dominant lateral variation in sound speed is confined to the upper few hundred meters and has timescales of tens of minutes driven by internal waves. Any net lateral bias in the GPS-A position estimate is practically removed by collecting data for tens of hours to days. In summary, the GPS-A method is capable of ±1.5-cm positioning with 24 h of data and likely of subcentimeter-level precision after 3 to 4 days (Chadwell & Spiess 2008, Fujita et al. 2006, Gagnon et al. 2005).

Continuous Pressure-Sensor Monitoring of Vertical Motions

Another proven seafloor geodetic technique measures vertical seafloor displacements by sensing the resulting change in seawater pressure that occurs at the shifted seabed (**Figure 4*a***). Changes in atmospheric pressure are routinely used to determine elevation in a variety of terrestrial navigation applications, though the relatively low density of the atmosphere and its oscillations from environmental forcing severely limit the use of barometers as geodetic sensors. Seawater is much denser, with pressure increasing by approximately 1 atm for every 10-m increase in depth. A 1-cm change in depth generates a significant, measureable change in pressure.

Presently, the best technology uses a Bourdon tube, a tube in the shape of the letter J. The top of the long axis of the tube is open to seawater, while the end on the short axis is capped. A small quartz strain gauge is attached at the capped end and extends across to the middle of the long axis. An increase in seawater pressure slightly straightens the tube, exerting a proportional strain that is measured as a corresponding change with the frequency of the quartz oscillator. This configuration can detect the equivalent of a few millimeters of height change over a wide range of pressures from 1 atm at the surface to extreme high pressures at 6,000-m depths. Short, sharp shifts are easily captured, but small, slow displacements are more challenging. The difficulty arises because the gauges have an inherent, unpredictable drift of approximately 8 cm/yr and because the deformation signal can easily be produced by a variety of natural pressure signals with similar magnitude and time constants (Polster et al. 2009).

On the deep seafloor below the influence of waves and other near-surface processes, pressure variations result from tides, tsunamis, and regional or mesoscale atmospheric/oceanographic changes. One approach to isolate a gradual deformation signal is to place a reference benchmark outside the region of expected deformation and make campaign-style relative depth measurements at an array of benchmarks. Pressure is recorded at the benchmark, and the gauges are moved using

a remotely operated vehicle into the active field, where pressure is recorded at additional monuments before returning to the far-field reference mark. The depth difference is calculated between the reference and benchmarks in the active field. Over the few hours to days of the survey, the gauge has negligible drift. Tidal signals can be removed by using a predictive model or, preferably, by continuously recording pressure with an independent, autonomous gauge deployed on the seafloor during the survey.

An active area of research is the development of a drift-free or self-calibrated pressure gauge, with the goal of reducing instrument drift from ~8 cm/yr to 1 cm/yr or better. Sasagawa & Zumberge (2013) have developed a calibration system that is deployed with the gauge. An initial test of the device at a depth of over 600 m, lasting 104 days, kept the gauge uncertainty to 1.3 cm.

Repeat Active-Source Sonar and Seismic Surveying

Ranging with sound is also used in multibeam mapping systems to collect soundings (depths) in several-kilometer-wide swaths of the ocean floor below a transiting ship (**Figure 4*b***). In the deep ocean, depth resolution is ~15 m and the size of the signal footprint is ~70 m. Repeat bathymetric mapping from ships can capture only the largest seafloor displacements associated with edifice

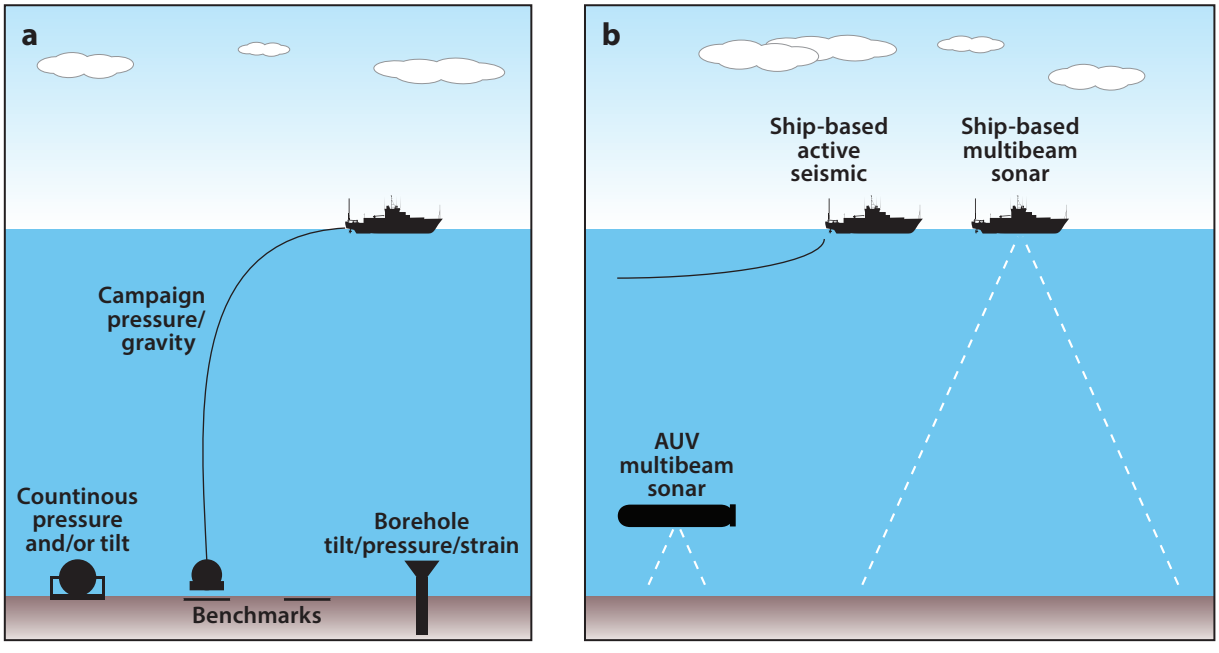

Figure 4

Schematic diagrams of a range of methods for seafloor measurements of seafloor displacements, tilt, gravity changes, and strain. (*a*) Pressure sensors, which can be deployed in infrequent campaigns or in continuous and cabled installations, detect vertical seafloor motions. Gravity measurements are sensitive to both vertical motions and subsurface mass redistributions. Ocean drilling boreholes can be instrumented with tiltmeters, strainmeters, and fluid pressure sensors. (*b*) Ship-based sonar can obtain bathymetric maps, which can be differenced for change measurements on the order of several meters. Sonar from autonomous underwater vehicles (AUVs) allows for higher-resolution bathymetry. Active-source seismic exploration from ships (sometimes aided by cabled seafloor geophone arrays) provides 4D time-lapse images of subsurface deformation.

collapse, mid-ocean ridge eruptions, and subduction earthquake–related fault ruptures (Fujiwara et al. 2011). Higher-resolution mapping is possible from an autonomous or towed underwater vehicle operated tens of meters above the seafloor (e.g., Caress et al. 2012). A precisely navigated underwater vehicle can obtain seafloor bathymetric surveys at centimeter-level resolution by combining synthetic aperture interferometry and multibeam processing techniques (Asada & Ura 2010). Interferometric sonar provides enhanced precision of bathymetric measurements, relying on two or more vertically spaced receiving elements that can determine the direction from which the signal was received in addition to the range distance (Geen 1998). Interferometric techniques from ships analogous to InSAR (i.e., interferometric synthetic aperture sonar, or InSAS) hold promise for meter- to decimeter-level resolution, and this is an area of active research, but to date there has been no practical demonstration.

Lower-frequency sound propagates into the seabed and can seismically image subsurface structure. The lower-frequency signals have longer wavelengths and reduced vertical resolution compared with multibeam sonars imaging the seafloor. Repeated active-source seismic surveys can be used to detect changes in travel times associated with changes in layer thickness and seismic velocity due to strain (e.g., Guilbot & Smith 2002, Hatchell & Bourne 2005). As seismic velocity depends on deformation and changing rock properties (e.g., anisotropic crack densities), interpretation and modeling of such data is complex (Hatchell & Bourne 2005).

Other Methods

Several additional techniques have been developed, but most of them have yet to be deployed in sufficient numbers or for sufficient durations to capture real geophysical deformation. The fiber-optic strain sensor times the propagation of a light pulse over a fiber-optical cable stretched across the seafloor (Zumberge 1997). It can detect movements of a few millimeters over cable lengths up to several hundred meters. Its primary advantage is that it is isolated from seawater sound speed variations that can affect acoustic ranging in hydrothermally active regions of the ocean, e.g., mid-ocean ridges.

Terrestrial sensors for measuring gravity and tilt have been adapted for seafloor use by enclosing them in air-filled, watertight vessels that maintain the internal air pressure at nominally 1 atm. A variety of relative gravimeters have been used on the seafloor (Zumberge et al. 2008). Short-baseline tilt sensors measure the tilt over the approximately 1-m-wide aperture of the sensor frame (Fabian & Villinger 2008). Although resolution approaches 0.1 μrad/day, long-term drift limits applications to concentrated strain events. Additionally, coupling of the instrument to the seafloor can be disturbed by water movement (Anderson et al. 1997, Tolstoy et al. 1998). A borehole tiltmeter to be deployed in Cascadia will avoid this source of spurious signal (J. McGuire, personal communication). Additionally, borehole pressure sensors can detect small fluid pressure changes associated with crustal strain from volcanic or faulting processes (Davis et al. 2004, 2011).

APPLICATIONS AND ACCOMPLISHMENTS OF SEAFLOOR GEODESY

Improving our understanding of the processes involved in plate tectonics and quantifying tectonic plate motions, intraplate strain, and earthquake cycle deformation at plate boundary faults provide a strong rationale to carry out precise geodetic measurement in general, but especially on the seafloor. Seafloor displacements associated with submarine volcanoes, landslides, and extraction or injection of fluids and gas represent additional important targets. Here we provide an overview of some results from seafloor geodesy during the past two decades.

The Juan de Fuca Plate: Plate Motion, Ridge Spreading, and Subduction

The Juan de Fuca plate represents a natural laboratory for seafloor geodetic studies of oceanic plate creation, motion, and subduction. It is subducting at a rate of ~40 mm/yr under western North America along the Cascadia subduction zone. A system of spreading ridges and transform faults bounds the plate to the west and south (**Figure 5*a***).

Starting in the early 1990s, acoustic ranging systems were deployed to measure horizontal extension across the 1-km-wide axial valley at the south Cleft segment of the Juan de Fuca Ridge. Whereas the long-term spreading rate established from seafloor magnetic lineations is 52 ± 1 mm/yr (Wilson 1993), the short-baseline measurements found no significant extension (with ~5 mm/yr uncertainty) across the axial valley during 1994–1999 and 2000–2003 (Chadwell et al. 1999, Chadwick & Stapp 2002). This suggests that spreading on the ridge axis occurs only episodically. Although no spreading could be measured at the rift valley, the velocity of a GPS-A station ~25 km east of the south Cleft ridge shows motion of the Juan de Fuca plate consistent with the magnetic lineation data (**Figure 5*b***) (Chadwell & Spiess 2008). Thus, similar to the earthquake cycle, involving many years of elastic shear stress accumulation relieved by seismic slip events, oceanic ridge spreading involves long periods of broadly distributed stress buildup relieved by relatively short-duration magmatic dike intrusions.

Two additional GPS-A stations on the Juan de Fuca plate, closer to the trench, are moving in the direction of the predicted plate motion, but at velocities less than predicted by the geologic plate motion model (**Figure 5*a***) (Spiess et al. 1998; D. Chadwell, unpublished results). This indicates either elastic or permanent deformation of the Juan de Fuca plate near the locked subduction thrust. Multiple GPS-A profiles across the plate margin are needed to determine the distribution of coupling of the shallow portion of the Cascadia megathrust.

Subduction Zone Earthquake Cycle Deformation

Earthquakes, as large as $M_w > 9$ with tens of meters of slip, accommodate most of the plate convergence at subduction zones. Although most subduction megathrusts appear to be interseismically locked at depths shallower than ~50 km, some are found to be partially uncoupled and accommodate part of their slip budget by aseismic creep. On-land geodetic studies can help resolve the down-dip edge of the locked zone, but as most of the subduction thrust is located offshore, the resolution of such studies is limited and the degree of coupling in the near-trench region cannot be determined (Bürgmann et al. 2005, Loveless & Meade 2011, McCaffrey et al. 2013). Studies of the distribution and frequency content of subduction earthquakes suggest a complex assemblage of seismic and aseismic patches and areas that are conditionally stable; i.e., they are capable of both aseismic slip and coseismic rupture (**Figure 2**) (Lay et al. 2012, Scholz 1998). Time-dependent subduction slip between, just before, and immediately after earthquake ruptures has been observed (Schwartz & Rokosky 2007). In situ monitoring of such slip is likely to improve our understanding of subduction earthquake cycles, precursory slip transients, and tsunami earthquakes.

To date, seafloor geodetic studies have targeted subduction zones off Peru (Gagnon et al. 2005), Costa Rica (Davis et al. 2011), the New Hebrides in the southwest Pacific (Ballu et al. 2013), and Japan. Gagnon et al. (2005) obtained interseismic velocities of two stations located on the accretionary complex overlying the subducting oceanic Nazca plate offshore Peru. The observed velocities relative to the overriding South American plate are within 20% of the total plate convergence rate. These high rates support models of a fully coupled subduction thrust from a depth of 2 to 40 km (Gagnon et al. 2005). The strong locking at shallow depths suggests that earthquakes rupturing the megathrust in this section of the Peru-Chile trench may have

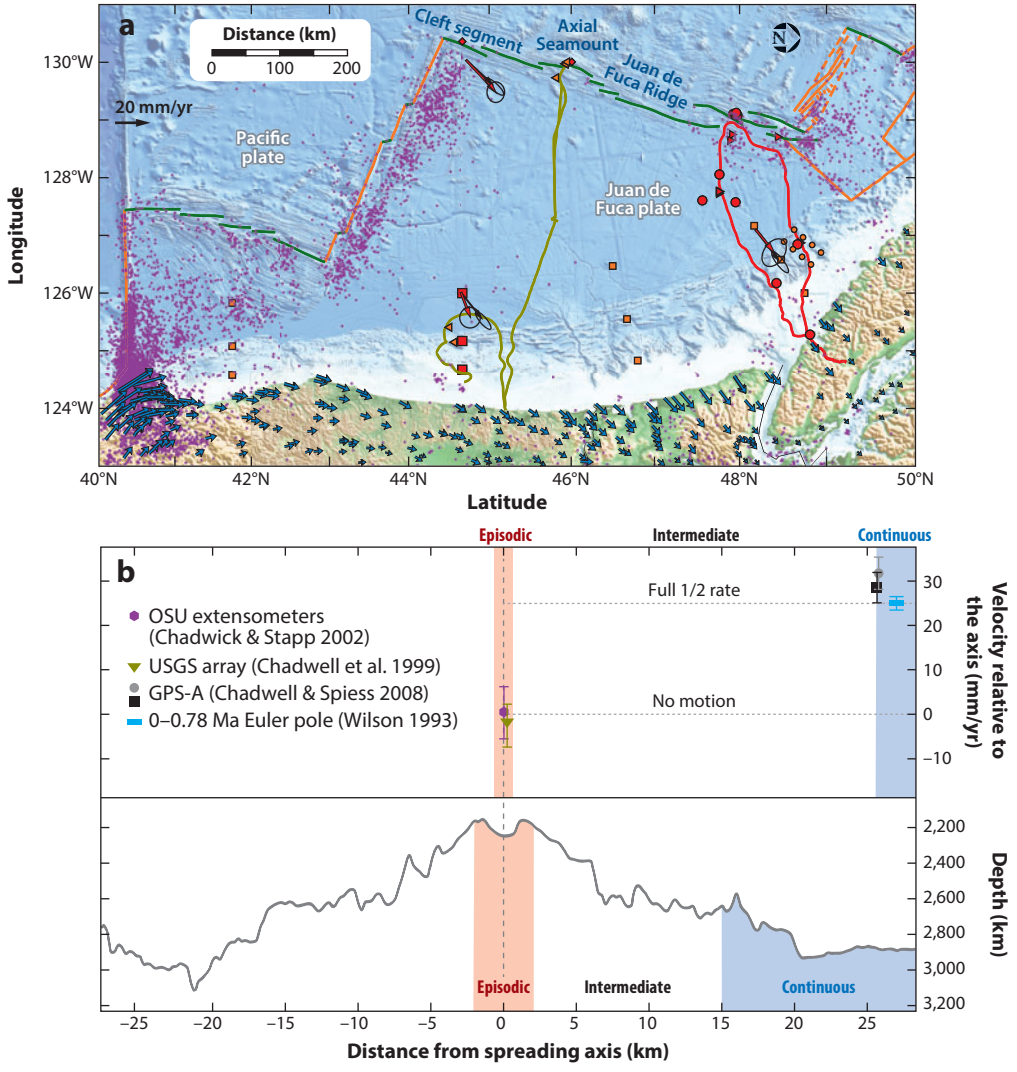

Figure 5

Seafloor geodetic measurements of plate motion, mid-ocean ridge spreading, and subduction-related deformation of the Juan de Fuca plate. (*a*) Map of existing and in-progress measurements. Three GPS-A velocities (*red arrows*) are compared with geologic plate motion of the Juan de Fuca plate with respect to stable North America (Wilson 1993) (*black arrows*). Northeast-directed GPS velocities along the coast (*blue arrows*) reflect the broad interseismic elastic strain accumulation across the Cascadia subduction zone (McCaffrey et al. 2013). Red and orange squares are recently funded and proposed GPS-A profiles, respectively, across the locked subduction thrust. Red triangles are existing Ocean Drilling Program boreholes instrumented with formation and seafloor pressure sensors (Davis et al. 2004), and red circles are seafloor pressure sensors, on or near the NEPTUNE Canada cable (*red line*) (E. Davis, personal communication). A borehole tiltmeter, seafloor geodetic benchmarks, and a pressure-sensor array (*orange circles*) are to contribute additional data in real time via the Canadian cable system (*red line*) (J. McGuire, personal communication). Orange triangles mark nodes instrumented with pressure sensors of a new seafloor cable system off Oregon (*green line*; Ocean Observatories Initiative Regional Scale Nodes). Purple dots are $M > 3$ earthquakes, dark yellow lines are spreading ridges, and orange lines are oceanic transform faults. (*b*) Summary of seafloor measurements of extension across the Cleft segment of the Juan de Fuca Ridge (modified from Chadwell & Spiess 2008). Velocities away from the rift and bathymetry are shown as a function of distance from the ridge axis. Whereas acoustic direct-path ranging systems across the ridge by USGS and Oregon State University (OSU) did not observe a spreading signal, far-field GPS-A measurements are consistent with the tectonic motion of the Juan de Fuca plate.

high coseismic slip up to near the trench. Such shallow earthquake slip produces substantial uplift of the seafloor near the trench and is likely to result in particularly large tsunamis (Satake & Tanioka 1999), like the 1996 M_w 7.5 earthquake off Peru, located ~200 km north of the GPS-A profile.

Comprehensive seafloor monitoring of subduction zone deformation and hazard has progressed most impressively off Japan. Complementing a >1,300-station continuous GPS network onshore, tens of GPS-A stations have been established along the east coast of Japan (**Figure 6*a***). The data gathered at these stations provide valuable information about the distribution of interseismic coupling, earthquake displacements, and postseismic deformation. Two stations deployed by the Japan Coast Guard (MYGI and MYGW) are located near the rupture zones of both the 2005 *M* 7.2 Miyagi-oki earthquake and the 2011 *M* 9 Tohoku earthquake (**Figure 6*b***). Westward motions prior to the 2005 event document strong interseismic coupling below these stations. The sites shifted eastward by several centimeters during the 2005 earthquake (Matsumoto et al. 2006), and MYGW continued moving eastward for another year, indicative of postseismic afterslip (Sato et al. 2011b). Interseismic coupling was reestablished in 2007, but it appears that the degree of coupling was somewhat less than before 2005 (see 2002–2005 versus 2006–2011 velocity vectors of station MYGI in **Figure 6*b***). Whereas interseismic coupling off Miyagi is strong, the slow motion of station FUKU approximately 150 km to the south suggests a very weakly coupled subduction thrust along this section of the megathrust (Matsumoto et al. 2008). Inferences of the first-order distribution of coupling from the seafloor GPS-A stations are consistent with results from inversions of land-based GPS stations (Hashimoto et al. 2009, Loveless & Meade 2011) and from the distribution and rate of repeating microearthquakes on the subduction thrust (Uchida & Matsuzawa 2013).

A network of continuously operating ocean-bottom pressure sensors provided valuable information about the dynamic deformation processes in the subduction system leading up to the 2011 Tohoku earthquake (Ohta et al. 2012). The earthquake was preceded by several months of accelerated seismicity, including small repeating earthquakes indicative of nearby fault creep (Kato et al. 2012, Uchida & Matsuzawa 2013). Two days before the mainshock, an *M* 7.3 event occurred within a few tens of kilometers of the hypocenter. The pressure-sensor data provide detailed information about deformation from the foreshock and its afterslip, which continued at a rapid pace up to the *M* 9 mainshock (**Figure 7*a***) (Ohta et al. 2012). The pattern of uplift and subsidence during the postseismic period supports models of the afterslip reaching to near the *M* 9 hypocenter (**Figure 7*b***). The spatial expansion of the aftershock zone of the *M* 7.3 event also suggests southward propagation of the slow-slip zone toward the mainshock hypocenter (Kato et al. 2012). It appears that this precursory activity was part of a progressive unfastening process preceding the event, for several months and possibly years (Kato et al. 2012, Uchida & Matsuzawa 2013, Ito et al. 2013). However, the continuous pressure-sensor measurements do not reveal resolvable short-term precursory deformation near the Tohoku earthquake nucleation zone in the hours or minutes before the rupture (Hino et al. 2013).

The 2011 *M* 9 Tohoku earthquake produced horizontal displacements as large as 31 m at seven GPS-A stations near the coseismic rupture (**Figure 6*c***) and resulted in a devastating tsunami from large-scale seafloor uplift near the trench (Kido et al. 2011, Sato et al. 2011a). Six continuously operating pressure gauges also captured the coseismic deformation of the earthquake, providing evidence for uplift of more than 5 m near the trench (Ito et al. 2011). The seafloor geodetic data add particularly valuable constraints in inversions for the submarine slip distribution of the coseismic rupture (e.g., Iinuma et al. 2012). Relatively imprecise horizontal positioning of two of the pressure gauges supports horizontal motions of more than 50 m within 20 km of the trench (**Figure 8*b***) (Ito et al. 2011). Such large displacements near the trench are also indicated by

analysis of repeated multibeam bathymetric surveys obtained in 1999, 2004, and 2011 (Fujiwara et al. 2011). Differencing of pre- and postearthquake bathymetric data reveals substantial changes, indicating horizontal trenchward motions of the accretionary prism of as much as 50 m and total uplift of the seafloor by approximately 10 m right up to the trench (**Figure 8*a***). Kodaira et al. (2012) used seismic reflection data collected along the same line to image changes in the subsurface structure related to the earthquake rupture. Qualitative comparison of a profile taken in 1999 with

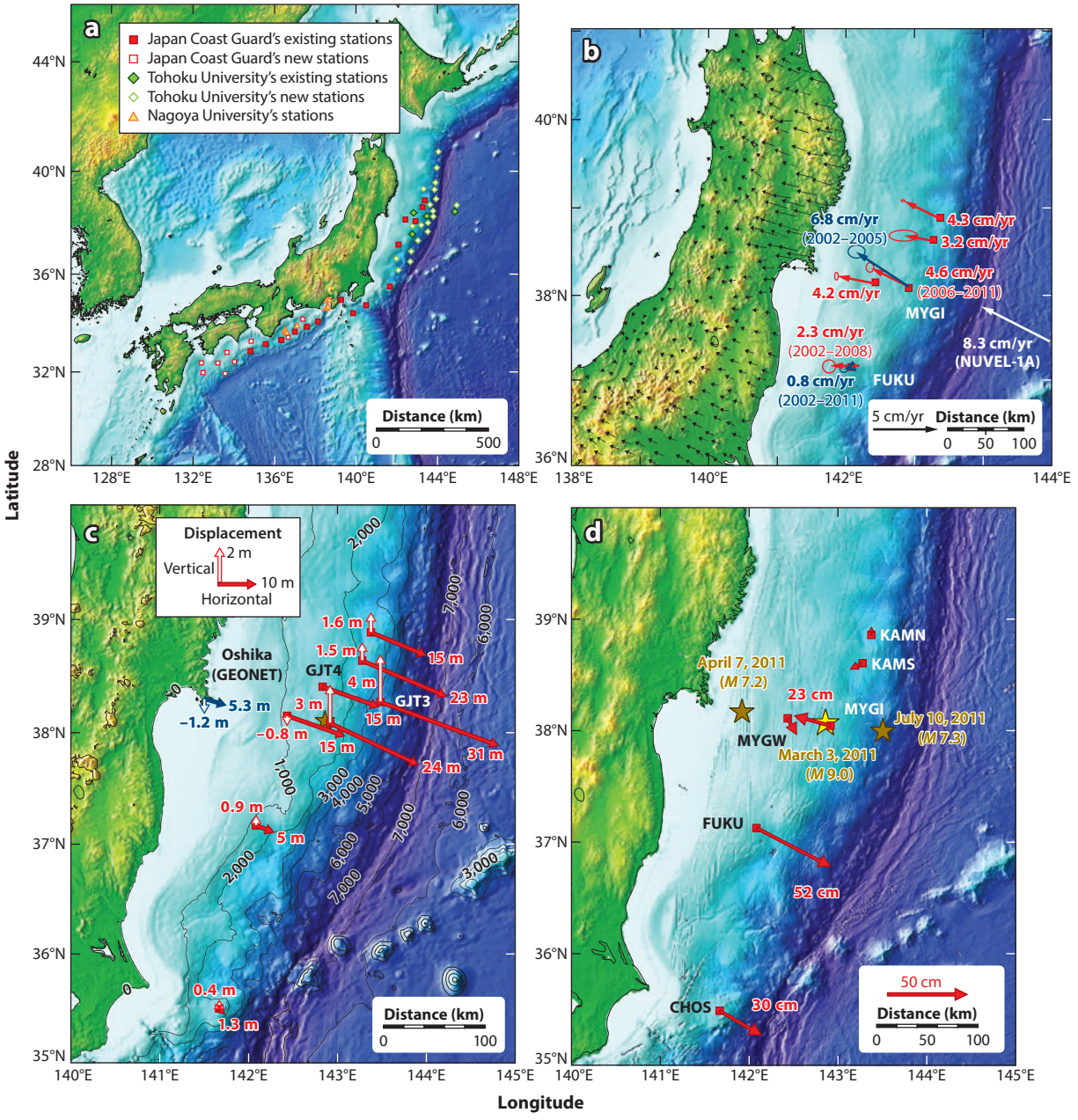

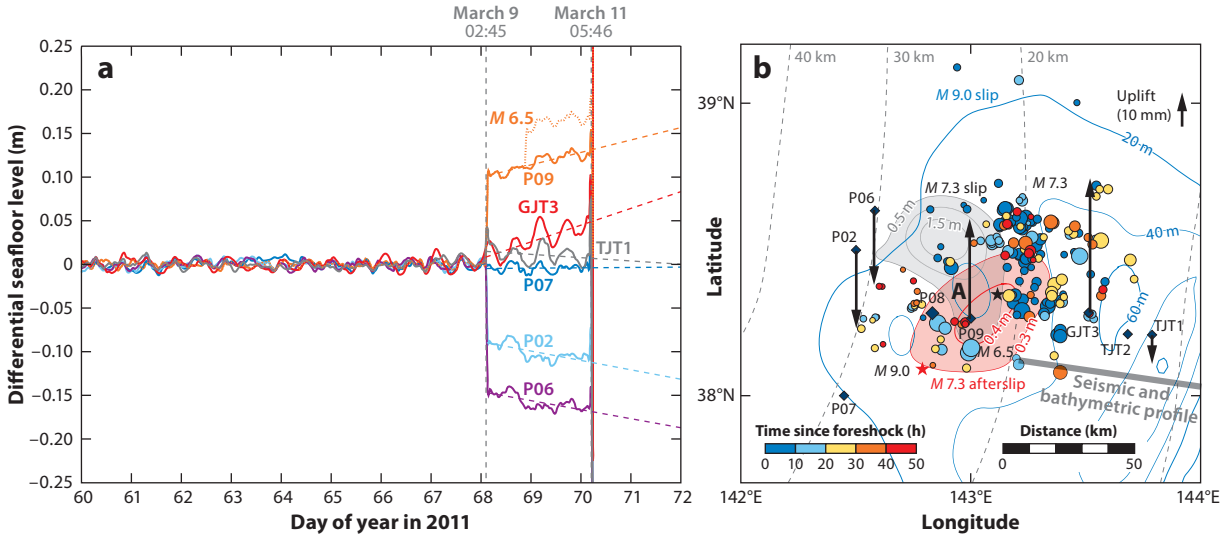

Figure 7

Coseismic and postseismic slip of the March 9, 2011, *M* 7.3 foreshock of the March 11 *M* 9 Tohoku earthquake from pressure-sensor time series and onshore GPS displacements (modified from Ohta et al. 2012 and R. Hino, personal communication). (*a*) Twelve-day time series of pressure sensors relative to station P08, spanning the foreshock and mainshock. Note the offset of P09 due to a nearby *M* 6.5 event. (*b*) Gray and red shaded contours show the coseismic and afterslip distributions of the *M* 7.3 foreshock, respectively. The blue contours indicate 20-m intervals of the Tohoku earthquake slip distribution from Iinuma et al. (2012). The black and red stars are the epicenters of the foreshock and Tohoku mainshock, respectively. Circles show aftershocks of the *M* 7.3 event color-coded by time since the foreshock. Dashed contours show the depth to the megathrust at 10-km intervals. The gray shaded bar shows the location of the bathymetric and seismic profile shown in **Figure 8**.

one collected 11 days after the earthquake (**Figure 8*c***) shows an intensively deformed and uplifted sedimentary sequence near the trench. Kodaira et al. (2012) interpreted this as a zone of multiple fault thrust splays, showing that the Tohoku earthquake rupture reached the seafloor. A narrow zone of subsidence just to the west of the uplift zone is interpreted as a slump. The large vertical seafloor displacements near the trench enhanced the catastrophic tsunami that resulted from the earthquake.

Figure 6

Seafloor GPS-A measurements of subduction zone deformation off Japan. (*a*) Existing and new GPS-A stations deployed by Japan Coast Guard, Tohoku University, and Nagoya University (M. Sato, personal communication). (*b*) Interseismic velocities in the North America reference frame measured during 2001–2011 (Sato et al. 2013). Error ellipses represent one-standard-deviation confidence regions of the estimated velocities. The two velocities for station MYGI are for before and after the 2005 *M* 7.2 Miyagi-oki earthquake. The two velocities for station FUKU reflect an apparent offset or rate change around 2008, possibly associated with extensive postseismic afterslip of the 2008 *M* 6.9 Fukushima-oki earthquake. The white velocity vector shows the Pacific–North America convergence rate from the geologic plate motion model (DeMets et al. 1994). Black arrows show velocities of terrestrial continuous GPS stations of the GPS Earth Observation Network (GEONET) operated by the Geospatial Information Authority of Japan. (*c*) Coseismic seafloor displacements (*red arrows*) of the 2011 *M* 9.0 Tohoku earthquake from GPS-A measurements by Japan Coast Guard (Japan Coast Guard 2011, Sato et al. 2011a) and Tohoku University (GJT3, GJT4) (Kido et al. 2011). For comparison, the displacement of a coastal GEONET station (*blue arrows*) with the largest measured coseismic offset is shown (Ozawa et al. 2011). (*d*) Postseismic motions of seafloor stations during a ~10-month period following the earthquake (Japan Coast Guard 2012). The dark yellow and orange stars show the epicenters of the mainshock and two large aftershocks, respectively. All depths are in meters.

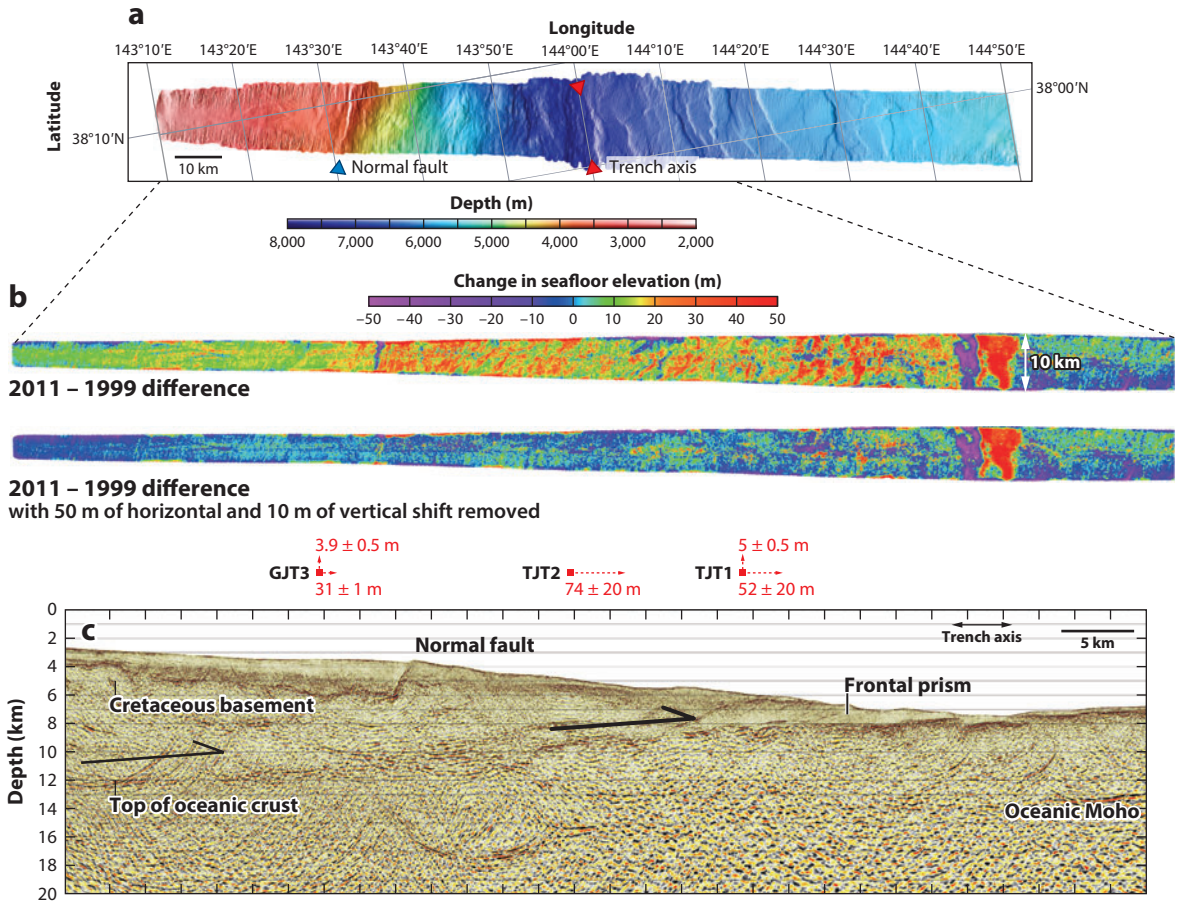

Figure 8

Coseismic vertical and horizontal displacements of the Tohoku earthquake near the trench (modified from Fujiwara et al. 2011, Ito et al. 2011, Kodaira et al. 2012). (*a*) Bathymetry and bathymetric change from multibeam bathymetric surveys acquired in 1999 and after the earthquake. By shifting the bathymetry obtained after the earthquake landward by 50 m and downward by 10 m, the apparent difference from the 1999 data is greatly reduced (Kodaira et al. 2012). (*b*) Red arrows show horizontal and vertical displacements measured with GPS-A (GJT3) and standard GPS with acoustic ranging and ocean-bottom pressure sensors (TJT1, TJT2) near the seismic profile (Ito et al. 2011). See **Figure 7** for station and profile locations. (*c*) Seismic reflection image (no vertical exaggeration) of the accretionary prism from data collected 11 days after the earthquake (Kodaira et al. 2012). Qualitative comparison of seismic reflection data from 1999 and after the earthquake reveals substantial deformation and mass transport in the trench axis.

Resurveys of five GPS-A stations within about 10 months of the first occupation after the earthquake revealed postseismic transient motions (**Figure 6*d***) (Japan Coast Guard 2012). Stations FUKU and CHOS to the south of the coseismic rupture zone moved trenchward by several decimeters, consistent with substantial afterslip induced on aseismically slipping portions of the megathrust below this area. Surprisingly, station MYGI moved ∼23 cm toward shore. Explanation of this displacement requires either postseismic backward (normal) slip on the megathrust to recover overshoot during the rupture (Ide et al. 2011) or surface motion due to viscous relaxation of coseismic stress changes in the underlying mantle asthenosphere (Wang et al. 2012).

In 2011, there were approximately 30 offshore GPS-A stations to monitor interseismic coupling and earthquake potential of the Nankai and Japan subduction zones. Twenty more GPS-A stations were installed along the Japan Trench in 2012, and nine new stations were added in the Nankai subduction zone (**Figure 6*a***). Also, a network of approximately 150 ocean-bottom pressure sensors and seismometers connected by fiber-optic cables for continuous monitoring of earthquakes, vertical motions, and tsunamis off northeast Japan is in development (Monastersky 2012), similar to existing smaller cabled systems in the Nankai trough area (Mikada & Asakawa 2008). Data from the enhanced seafloor geodetic networks are sure to provide new insights into the dynamics of active subduction zone systems.

The Growth and Collapse of Oceanic Volcanoes

A target of seafloor-geodetic investigations for more than two decades, Axial Seamount is a volcano on the Juan de Fuca Ridge (**Figure 5*a***), where additional magma supply from the Cobb hot spot enhances volcanic activity. The volcano features a large summit caldera and two rift zones extending to the north and south (**Figure 9*a***). Two eruptions in 1998 and 2011 occurred since geodetic monitoring began at Axial Seamount. The 1998 eruption along the south rift zone was preceded by extension and accompanied by contraction at an acoustic ranging site across the northern rift segment (Chadwick et al. 1999). The ranging and pressure measurements suggest pre-eruption extension and uplift across Axial Seamount followed by subsidence and contraction across the summit during the eruption. The 2011 eruption and summit subsidence also lasted for 6 days, but deflation associated with the 2011 eruption was less than in 1998 (**Figure 9*b***) (Chadwick et al. 2012). The data support a model of a relatively regular inflation-deflation cycle with precursory signals in the final minutes to hours as the dike intrusion nears the seafloor, allowing for possible forecasting and short-term prediction of future eruptions (Chadwick et al. 2012). Caress et al. (2012) differenced pre- and posteruption bathymetric surveys by an autonomous underwater vehicle with 1-m lateral resolution and 0.2-m vertical precision, to determine the extent and volume of the 2011 lava flows (**Figure 9*c***). The results show that the 2011 eruptive fissures in part reoccupied those from 1998 and prior eruptions. A cabled observatory and additional pressure-sensor sites will soon enhance seafloor geodetic monitoring of Axial Seamount (**Figure 5*a***), allowing for testing of these ideas in future eruptive episodes.

Kilauea Volcano on the Big Island of Hawaii is volcanically active and periodically undergoes rapid deformation and collapse of its southern edifice. Phillips et al. (2008) used an array of nine pressure sensors to characterize the offshore vertical deformation field of Kilauea's mobile south flank (**Figure 10*a***). The 2000–2004 measurements show up to 9 cm/yr of uplift on a large slump structure ~15 km southeast of the coastline (**Figure 10*b***). Elastic dislocation modeling of the uplift data shows that the observed deformation can be fit by rapid slip of nearly 30 cm/yr on a 25-km-wide, shallowly dipping fault plane at the base of the volcanic edifice. The results support a view of the south flank décollement system of Kilauea being active in large earthquake ruptures (Owen & Bürgmann 2006); in continuous, rapid aseismic slip (Phillips et al. 2008); in episodic slow slip transients (Brooks et al. 2006); and in catastrophic large-scale slope failures (Morgan et al. 2003).

Submarine Fluid Extraction and Injection

Extraction of oil and gas from submarine formations and injection of fluids and CO_2 for extraction enhancement or storage lead to redistribution of mass and deformation of the reservoir. Characterization of this deformation is important to optimize extraction/injection strategies

and to minimize damage to drilling infrastructure. Monitoring of offshore reservoir deformation employs time-dependent seismic imaging, pressure sensors, acoustic ranging, and gravimetric measurements.

Seismic waves refracting and reflecting in a reservoir and nearby rocks will have changing travel times during depletion, caused by both layer-thickness changes and changes in seismic velocity due to strain. Thus, time-lapse seismic reflection measurements allow for 4D seismic monitoring

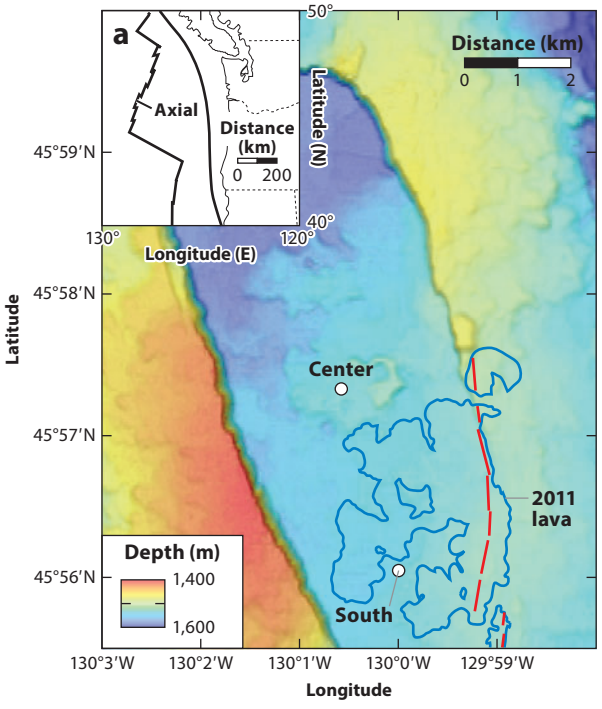

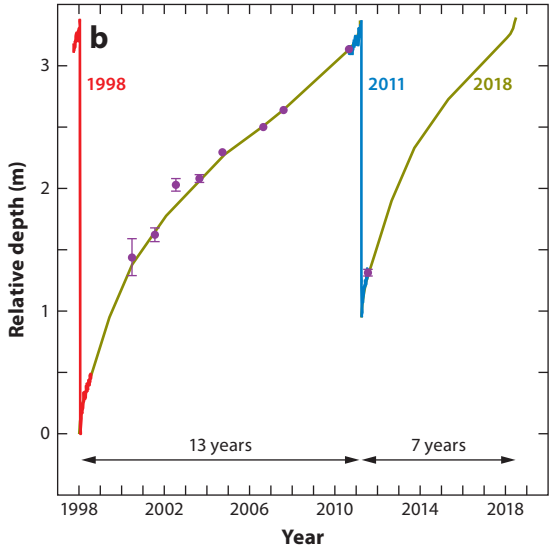

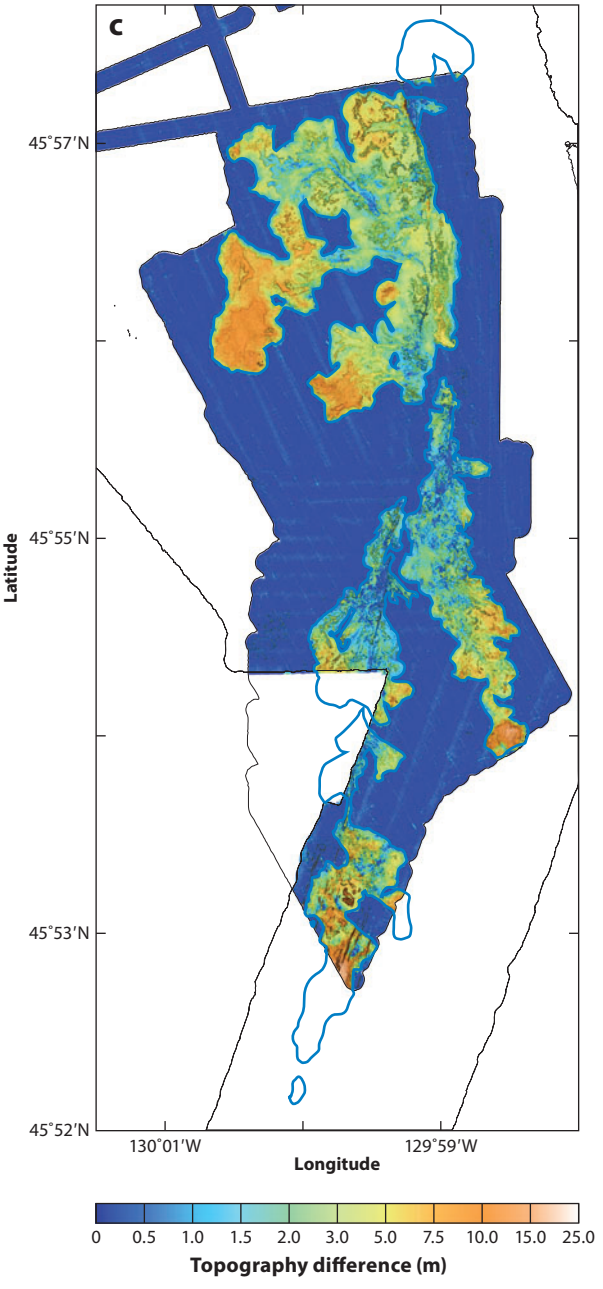

of deforming reservoirs (e.g., Guilbot & Smith 2002, Hatchell & Bourne 2005). The use of other wave types, such as surface waves and critically refracted compressional waves, enables a detailed look at the geomechanical response to deformation of the reservoir overburden in the near surface (Wills et al. 2008). **Figure 11** provides an example showing surface subsidence and seismic time-lapse time shifts resulting from reservoir compaction and overburden extension accompanying oil and gas production in the Dan field in chalk formations offshore Denmark, from 1988 to 2005 (Hatchell et al. 2007).

Acoustic ranging, pressure, and gravity measurements are considered low-cost alternative reservoir monitoring approaches, compared with seismic time-lapse techniques (Bourne et al. 2009). Bourne et al. (2009) described a networked acoustic ranging system that autonomously measures horizontal deformation over the compacting Ormen Lange gas/oil reservoir offshore Norway from hourly distance measurements among the networked stations. Gravity- and pressure-change data provide information about both vertical deformation and redistribution of mass below the seafloor associated with fluid extraction and injection (e.g., Alnes et al. 2011, Eiken et al. 2008). Eiken et al. (2008) used both pressure and gravity measurements to characterize the changing distribution of gas, oil, water, and porosity in the Troll field in the North Sea (**Figure 12**). An integrated pressure-gravity monitoring system has also been used in the Sleipner field in the North Sea where CO_2 is separated from natural gas, compressed, and reinjected into an underground saline aquifer. Once the contribution of elevation changes (measured with few-millimeter-level precision) and other factors (natural gas extraction and water intrusion in the reservoir) are accounted for, gravity-change measurements allow estimation of the density and thus the temperature of the sequestered CO_2 (Alnes et al. 2011, Nooner et al. 2007).

DISCUSSION

Enhanced seafloor deformation monitoring in the world's oceans will likely reveal a panoply of dynamic deformation processes of tectonic, volcanic, and nontectonic systems. The seafloor geodetic systems offshore northeast Japan provided extremely valuable constraints on preseismic, coseismic, and postseismic deformation associated with the March 11, 2011, *M* 9 Tohoku earthquake and have motivated expansion of seafloor deformation monitoring in Japan and along the Cascadia subduction zone. More research is also indicated with a focus on fast-spreading mid-ocean rift systems and oceanic transform faults. Oceanic transform faults accommodate much of their slip budget by aseismic slip, and larger events are commonly preceded by foreshock activity and are thus highly predictable (McGuire et al. 2012). Precise seafloor geodetic monitoring of oceanic transform faults will greatly illuminate their dynamic slip behavior (McGuire & Collins 2013).

The precision and accuracy of seafloor systems can likely be substantially improved in the future. For example, improvements in the kinematic GPS positioning of the surface vehicle and improved transponder positioning through further characterization and modeling of signal refraction in the

Figure 9

Deformation and lava flows at Axial Seamount (modified from Caress et al. 2012, Chadwick et al. 2012). (*a*) Bathymetric map of the summit caldera of Axial Seamount showing the locations of two continuously operating bottom pressure sensors (*white circles*). Blue and red lines indicate the partial extent of April 2011 lava flows and their eruptive vents. (*b*) Cycle of inflation and deflation at Axial Seamount from pressure-sensor data at the center site (Chadwick et al. 2012). Red and blue time series show abrupt deflation accompanying the 1998 and 2011 eruptions. Relative uplift between the 1998 measurements and the initiation of intereruption measurements using a mobile pressure recorder system (*purple dots*) is unknown. The dark yellow curve shows a time-predictable forecast scenario, assuming the next eruption occurs at a critical level of inflation. (*c*) Difference between pre- and posteruption bathymetry showing the thickness of 2011 lava flows (Caress et al. 2012).

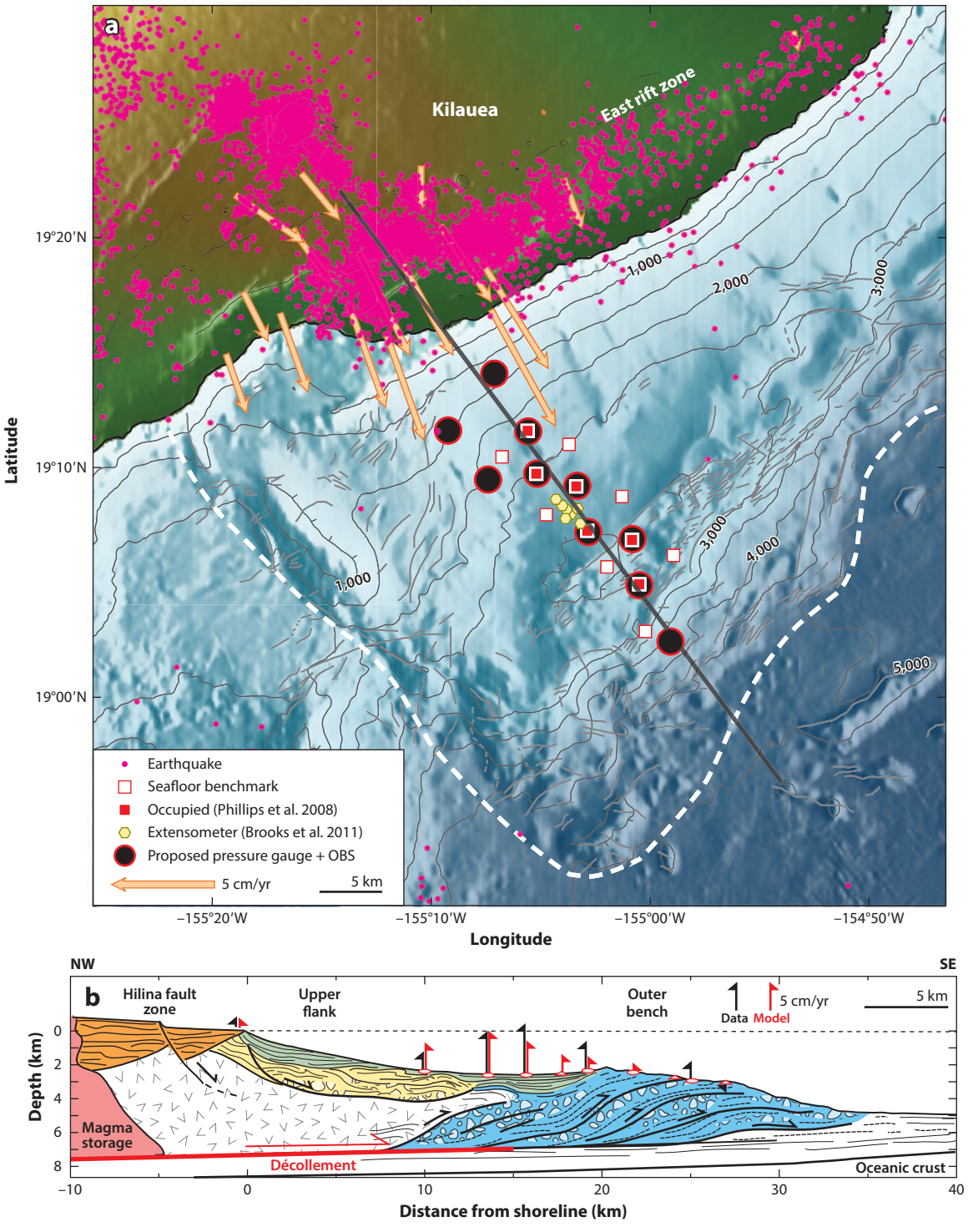

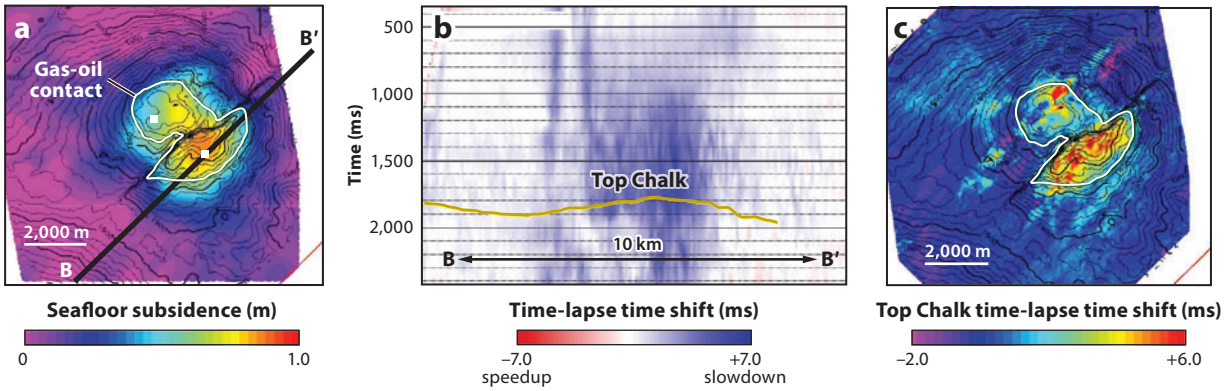

Figure 11

Subsidence and changes in seismic velocities in the compacting Dan field in the North Sea offshore Denmark, from 1988 to 2005 (modified from Hatchell et al. 2007 and P. Hatchell, personal communication). (*a*) Subsidence measured with echo sounding and GPS on two oil platforms (*white squares*). (*b*) Vertical cross-section of cross-correlation time shifts along B–B′ displayed in panel *a*. (*c*) Time-lapse time shifts observed from stacked seismic data at the top of the chalk reservoir shown by the dark yellow line in panel *b*. The time-lapse time shifts provide 4D mapping of strain and velocity changes in the reservoir.

oceans should push the precision of GPS-A horizontal positions to subcentimeter levels. More frequent measurements through permanent installations or by automated vehicles will improve the precision of deformation rates and the resolution of time-dependent processes. From an operational perspective, continuous GPS-A measurements remain challenging, requiring a sustained presence at the sea surface of a buoy or autonomous vehicle. Stable monumentation—for example, via drilled anchoring systems—will be necessary to ensure full precision of these measurements. For many of the processes targeted with seafloor geodesy, including volcano, fault, landslide, and reservoir monitoring, the availability of continuous, and often real-time, measurements is extremely advantageous. Thus, the use of cabled systems that provide power and continuously transmit data back to shore from a range of seafloor instruments is desirable.

One of the most severe challenges to the advance of seafloor geodesy is the high cost and logistics requirements for deploying and operating measurement systems. Research vessel costs exceeding $30,000/day can be forbidding. Thus, a key requirement for more widespread use of the techniques described in this article lies in the development of autonomous systems relying on buoys, autonomous surface and underwater vehicles, and other small-scale, lower-cost technologies. For example, autonomous, wave-powered surface vehicles could be used to carry out frequent GPS-A measurements of a network of transponder clusters at a fraction of the cost needed

Figure 10

Rapid submarine uplift of the south flank of Kilauea Volcano, Hawaii. (*a*) Map of geodetic network on the Hilina slump (*outlined by white dashed line*) on a topographic/bathymetric map (modified from Brooks et al. 2011 and J. Foster, personal communication). Orange arrows show 1997–2005 velocities of continuous GPS sites. Symbols indicate locations of existing and planned seafloor instrumentation including extensometers, pressure sensors, and ocean-bottom seismometers (OBS). (*b*) Cross-section through Kilauea's active submarine flank and uplift measurements (modified from Morgan et al. 2003, 2009; Phillips et al. 2008). The south flank is forced seaward by magmatic rift intrusions and gravitational spreading with aseismic slip along an active décollement (*red*) producing the GPS-measured seaward motion on land and uplift offshore. Uplift data (*black arrows*) and predicted uplift from an elastic fault model (*red arrows*) are from Phillips et al. (2008). All depths are in meters.

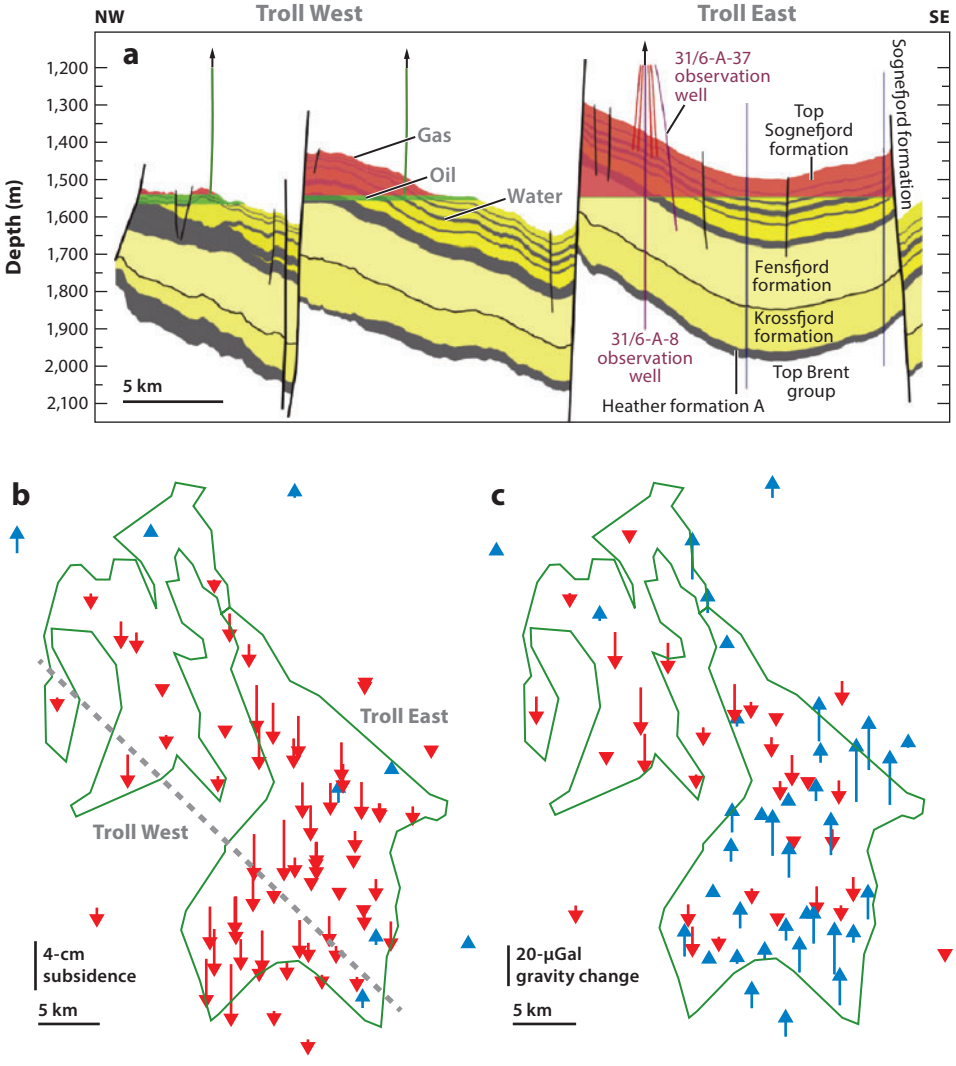

Figure 12

Elevation and gravity changes over Troll field, in the North Sea off Norway (modified from Eiken et al. 2008 and O. Eiken, personal communication). (*a*) NW–SE geologic cross-section across the field (see the gray dashed line in panel *b* for approximate location). (*b*) Seafloor elevation changes from pressure-sensor measurements spanning 2002 to 2005. The uncertainty (one standard deviation) of the depth differences is estimated at 1 cm. The green line outlines the hydrocarbon reservoir. (*c*) 2002–2005 gravity changes corrected for elevation changes, showing mass changes in the field. The one-standard-deviation uncertainty of gravity differences is 6.5 μGal. The gravity decrease in Troll West can be explained by oil production and a downward-moving gas-oil contact, whereas the gravity increase in Troll East is interpreted to be due to the influx of water from outside.

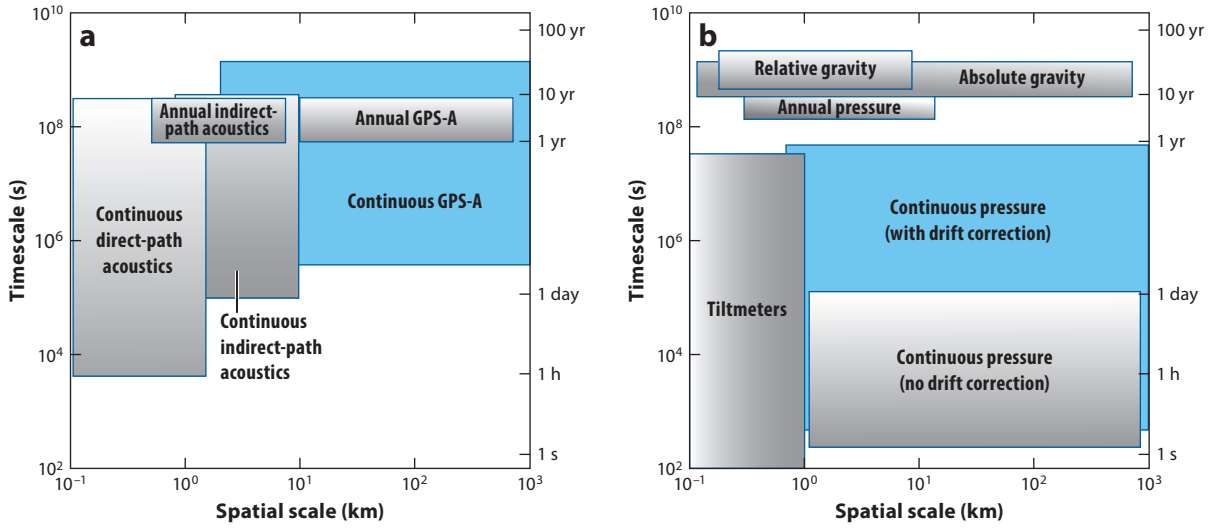

Figure 13

Comparison of horizontal and vertical accuracy of seafloor geodetic methods over a range of spatial and temporal scales. The log-log plots illustrate the ability of various seafloor geodetic sensors to resolve a 1-cm displacement over the spatial and temporal scales specified by labeled boxes in the plots. (*a*) Continuous GPS-A measurements (*blue box*) promise substantially improved temporal resolution of horizontal positioning. (*b*) Continuous pressure measurements with drift corrections provide increased long-term coverage of vertical motions.

to commit a research vessel to such an effort. Autonomous underwater vehicles are capable of providing many operations and maintenance activities on the seafloor. Assuming continued progress in the development of increasingly precise and cost-efficient seafloor geodetic monitoring tools, we envision a technological and scientific revolution.

The advent of continuous measurements in space-based, subaerial geodesy improved temporal resolution and both understanding and reduction of positioning errors. A similar evolution is underway in seafloor geodesy (**Figure 13**). Most seafloor geodetic sensors are easily configured for continuous measurements, including pressure and direct- and indirect-path acoustics. Cabled sensors offer the additional advantage of practically unlimited power and real-time communications. Recent accomplishments, strong scientific rationale, and technical improvements in seafloor geodesy suggest that the field will advance rapidly during the next decade.

SUMMARY POINTS

1. Seafloor geodetic measurements of deformation, strain, tilt, and gravity changes are possible with precision comparable to that of terrestrial systems.
2. Submarine observations of mid-ocean ridge deformation document episodic dike intrusion cycles with components similar to the earthquake cycle.
3. Seafloor measurements of earthquake cycle deformation off northeast Japan are revealing unique information about interseismic coupling, pre-earthquake slip transients, >50-m near-trench megathrust slip, and the rheology governing postseismic afterslip and viscous relaxation.

4. Seafloor geodesy using pressure sensors, gravimeters, and multibeam sonar and seismic time-lapse imaging allows for characterization of reservoir changes due to extraction or injection of fluids.
5. Recent technical advances and strong scientific rationale suggest rapid growth of seafloor geodetic applications.

FUTURE ISSUES

1. The development of seafloor geodetic systems relying on autonomous buoys and surface and subsurface vehicles will greatly enable more comprehensive monitoring efforts and reduce the cost of deployment.
2. Deployment of permanent benchmarks on the seafloor should extend positional time series beyond the life of a single seafloor sensor, analogous to the use of long-lasting monuments in subaerial geodesy.
3. Cabled systems will allow for continuous and real-time monitoring of subduction zone and volcanic systems and improve our understanding of their dynamics and associated hazards.
4. Self-calibrated pressure sensors should improve the detection of slow interseismic vertical motions.
5. Interferometric synthetic aperture sonar (InSAS) for high-resolution seafloor mapping and change detection may revolutionize seafloor geodesy, just as InSAR did in terrestrial geodesy.

DISCLOSURE STATEMENT

The authors are not aware of any affiliations, memberships, funding, or financial holdings that might be perceived as affecting the objectivity of this review.

ACKNOWLEDGMENTS

We thank Håvard Alnes, Ben Brooks, David Caress, Bill Chadwick, Earl Davis, Karen Douglas, Ola Eiken, James Foster, Toshiya Fujiwara, Paul Hatchell, Ryota Hino, Yoshihiro Ito, Deborah Kelley, Shuichi Kodaira, Thorne Lay, Jeff McGuire, Juli Morgan, Scott Nooner, Yusaku Ohta, Giora Proskurowski, Mariko Sato, David Sandwell, Glenn Sasagawa, and Mark Zumberge for providing valuable material and information for this review. We also thank Bill Chadwick, Emily Brodsky, and an anonymous reviewer for thoughtful comments. Many of the figures were prepared using the Generic Mapping Tools (Wessel & Smith 1998).

LITERATURE CITED

Alnes H, Eiken O, Nooner S, Sasagawa G, Stenvold T, Zumberge M. 2011. Results from Sleipner gravity monitoring: updated density and temperature distribution of the CO_2 plume. *Energy Procedia* 4:5504–11

Anderson G, Constable S, Staudigel H, Wyatt FK. 1997. A seafloor long-baseline tiltmeter. *J. Geophys. Res.* 102(B9):20269–85

Asada A, Ura T. 2010. *Full-swath bathymetric survey system with synthetic aperture and triangle-arrayed interferometric techniques for autonomous underwater vehicle*. Presented at OCEANS 2010, Sept. 20–23, Seattle, WA. doi: 10.1109/OCEANS.2010.5664359

Ballu V, Bonnefond P, Calmant S, Bouin MN, Pelletier B, et al. 2013. Using altimetry and seafloor pressure data to estimate vertical deformation offshore: Vanuatu case study. *Adv. Space Res.* 51:1335–51

Blum JA, Chadwell CD, Driscoll N, Zumberge MA. 2010. Assessing slope stability in the Santa Barbara Basin, California, using seafloor geodesy and CHIRP seismic data. *Geophys. Res. Lett.* 37:L13308

Bourne S, Hatchell P, Partridge S, Leaf C, Klemm H, et al. 2009. *An autonomous seafloor system for monitoring reservoir deformation*. Presented at EAGE Conf. Exhib., 71st, June 8, Amsterdam

Brooks BA, Foster JH, Bevis M, Frazer LN, Wolfe CJ, Behn M. 2006. Periodic slow earthquakes on the flank of Kilauea volcano, Hawaii. *Earth Planet. Sci. Lett.* 246:207–16

Brooks BA, Foster JH, McGuire JJ, Behn M. 2011. Submarine landslides and slow earthquakes: monitoring motion with GPS and seafloor geodesy. In *Encyclopedia of Complexity and System Science*, ed. W Lee, pp. 889–907. New York: Springer

Bürgmann R, Kogan MG, Steblov GM, Hilley G, Levin VE, Apel T. 2005. Interseismic coupling and asperity distribution along the Kamchatka subduction zone. *J. Geophys. Res.* 110:B07405

Bürgmann R, Thatcher W. 2013. Space geodesy: a revolution in crustal deformation measurements of tectonic processes. In *The Web of Geological Sciences: Advances, Impacts, and Interactions*, ed. ME Bickford, pp. 397–430. GSA Spec. Pap. 500. Boulder, CO: GSA

Caress DW, Clague DA, Paduan JB, Martin JF, Dreyer BM, et al. 2012. Repeat bathymetric surveys at 1-metre resolution of lava flows erupted at Axial Seamount in April 2011. *Nat. Geosci.* 5:483–88

Chadwell CD, Hildebrand JA, Spiess FN, Morton JL, Normark WR, Reiss CA. 1999. No spreading across the southern Juan de Fuca Ridge axial cleft during 1994–1996. *Geophys. Res. Lett.* 26:2525–28

Chadwell CD, Spiess FN. 2008. Plate motion at the ridge-transform boundary of the south Cleft segment of the Juan de Fuca Ridge from GPS-acoustic data. *J. Geophys. Res.* 113:B04415

Chadwell CD, Sweeney AD. 2010. Acoustic ray-trace equations for seafloor geodesy. *Mar. Geod.* 33:164–86

Chadwick WW Jr, Embley RW, Milburn HB, Meinig C, Stapp M. 1999. Evidence for deformation associated with the 1998 eruption of Axial Volcano, Juan de Fuca Ridge, from acoustic extensometer measurements. *Geophys. Res. Lett.* 26:3441–44

Chadwick WW Jr, Nooner SL, Butterfield DA, Lilley MD. 2012. Seafloor deformation and forecasts of the April 2011 eruption at Axial Seamount. *Nat. Geosci.* 5:474–77

Chadwick WW Jr, Stapp M. 2002. A deep-sea observatory experiment using acoustic extensometers: precise horizontal distance measurements across a mid-ocean ridge. *IEEE J. Ocean. Eng.* 27:193–201

Davis E, Becker K, Dziak R, Cassidy J, Wang K, Lilley M. 2004. Hydrological response to a seafloor spreading episode on the Juan de Fuca ridge. *Nature* 430:335–38

Davis E, Heesemann M, Wang K. 2011. Evidence for episodic aseismic slip across the subduction seismogenic zone off Costa Rica: CORK borehole pressure observations at the subduction prism toe. *Earth Planet. Sci. Lett.* 306:299–305

DeMets C, Gordon RG, Argus DF, Stein D. 1994. Effect of recent revisions to the geomagnetic reversal time scale and estimates of current plate motions. *Geophys. Res. Lett.* 21:2191–94

Eiken O, Stenvold T, Zumberge M, Alnes H, Sasagawa G. 2008. Gravimetric monitoring of gas production from the Troll field. *Geophysics* 73:WA149–54

Fabian M, Villinger H. 2008. Long-term tilt and acceleration data from the Logatchev hydrothermal vent field, Mid-Atlantic Ridge, measured by the Bremen Ocean Bottom Tiltmeter. *Geochem. Geophys. Geosyst.* 9:Q07016

Fox CG. 1993. Five years of ground deformation monitoring on Axial Seamount using a bottom pressure recorder. *Geophys. Res. Lett.* 20:1859–62

Fujimoto H, Koizumi K, Osada Y, Kanazawa T. 1998. Development of instruments for seafloor geodesy. *Earth Planets Space* 50:905–11

Fujita M, Ishikawa T, Mochizuki M, Sato M, Toyama S, et al. 2006. GPS/acoustic seafloor geodetic observation: method of data analysis and its application. *Earth Planets Space* 58:265–75

Fujiwara T, Kodaira S, No T, Kaiho Y, Takahashi N, Kaneda Y. 2011. The 2011 Tohoku-oki earthquake: displacement reaching the trench axis. *Science* 334:1240

Gagnon KL, Chadwell CD, Norabuena E. 2005. Measuring the onset of updip locking in the Peru-Chile Trench at 12°S from GPS and acoustic measurements. *Nature* 434:205–8

Geen M. 1998. *Applications of interferometric swath bathymetry*. Presented at OCEANS '98, Sept. 28–Oct. 1, Nice, Fr. doi: 10.1109/OCEANS.1998.724411

Guilbot J, Smith B. 2002. 4D-constrained depth conversion for reservoir compaction estimation. Application to the Ekofisk field. *Lead. Edge* 21:302–8

Hashimoto C, Noda A, Sagiya T, Matsu'ura M. 2009. Interplate seismogenic zones along the Kuril-Japan trench inferred from GPS data inversion. *Nat. Geosci.* 2:141–44

Hatchell P, Bourne S. 2005. Rocks under strain: strain-induced time-lapse time shifts are observed for depleting reservoir. *Lead. Edge* 24:1222–25

Hatchell P, Jorgensen O, Gommesen L, Stammeijer J. 2007. Monitoring reservoir compaction from subsidence and time-lapse timeshifts in the Dan field. *SEG Tech. Progr. Expand. Abstr.* 26:2867–71

Hino R, Inazu D, Ohta Y, Ito Y, Suzuki S, et al. 2013. Was the 2011 Tohoku-oki earthquake preceded by aseismic preslip? Examination of seafloor vertical deformation data near the epicenter. *Mar. Geophys. Res.* doi: 10.1007/s11001-013-9208-2

Ide S, Baltay A, Beroza GC. 2011. Shallow dynamic overshoot and energetic deep rupture in the 2011 M_w 9.0 Tohoku-oki earthquake. *Science* 332:1426–29

Iinuma T, Hino R, Kido M, Inazu D, Osada Y, et al. 2012. Coseismic slip distribution of the 2011 off the Pacific Coast of Tohoku Earthquake (M9.0) refined by means of seafloor geodetic data. *J. Geophys. Res.* 117:B07409

Ito Y, Hino R, Kido M, Fujimoto H, Osada Y, et al. 2013. Episodic slow slip events in the Japan subduction zone before the 2011 Tohoku-oki earthquake. *Tectonophysics* 600:14–26

Ito Y, Tsuji T, Osada Y, Kido M, Inazu D, et al. 2011. Frontal wedge deformation near the source region of the 2011 Tohoku-oki earthquake. *Geophys. Res. Lett.* 38:L00G05

Japan Coast Guard. 2011. Seafloor movements by seafloor geodetic observations before and after the 2011 off the Pacific Coast of Tohoku earthquake. *Rep. Coord. Comm. Earthq. Predict.* 86:284–93 (In Japanese)

Japan Coast Guard. 2012. Seafloor movements obtained by seafloor geodetic observations after the 2011 off the Pacific Coast of Tohoku earthquake. *Rep. Coord. Comm. Earthq. Predict.* 88:150–54 (In Japanese)

Kato A, Obara K, Igarashi T, Tsuruoka H, Nakagawa S, Hirata N. 2012. Propagation of slow slip leading up to the 2011 M_w 9.0 Tohoku-oki earthquake. *Science* 335:705–8

Kido M, Osada Y, Fujimoto H, Hino R, Ito Y. 2011. Trench-normal variation in observed seafloor displacements associated with the 2011 Tohoku-oki earthquake. *Geophys. Res. Lett.* 38:L24303

Kodaira S, No T, Nakamura Y, Fujiwara T, Kaiho Y, et al. 2012. Coseismic fault rupture at the trench axis during the 2011 Tohoku-oki earthquake. *Nat. Geosci.* 5:646–50

Lay T, Kanamori H, Ammon CJ, Koper KD, Hutko AR, et al. 2012. Depth-varying rupture properties of subduction zone megathrust faults. *J. Geophys. Res.* 117:B04311

Loveless JP, Meade B. 2011. Spatial correlation of interseismic coupling and coseismic rupture extent of the 2011 $M_w = 9.0$ Tohoku-oki earthquake. *Geophys. Res. Lett.* 38:L17306

Matsumoto Y, Fujita M, Ishikawa T, Mochizuki M, Yabuki T, Asada A. 2006. Undersea co-seismic crustal movements associated with the 2005 Off Miyagi Prefecture earthquake detected by GPS/acoustic seafloor geodetic observation. *Earth Planets Space* 58:1573–76

Matsumoto Y, Ishikawa T, Fujita M, Sato M, Saito H, et al. 2008. Weak interplate coupling beneath the subduction zone off Fukushima, NE Japan, inferred from GPS/acoustic seafloor geodetic observation. *Earth Planets Space* 60:e9–12

McCaffrey R, King RW, Payne S, Lancaster M. 2013. Active tectonics of northwestern US inferred from GPS-derived surface velocities. *J. Geophys. Res. Solid Earth* 118:709–23

McGuire JJ, Collins JA. 2013. Millimeter-level precision in a seafloor geodesy experiment at the Discovery transform fault, East Pacific Rise. *Geochem. Geophys. Geosyst.* 14:4392–402

McGuire JJ, Collins JA, Gouedard P, Roland E, Lizarralde D, et al. 2012. Variations in earthquake rupture properties along the Gofar transform fault, East Pacific Rise. *Nat. Geosci.* 5:336–41

Mikada H, Asakawa K. 2008. *Development of Japanese scientific cable technology*. Presented at OCEANS 2008, Sept. 15–18, Quebec City. doi: 10.1109/OCEANS.2008.5151942

Monastersky R. 2012. The next wave. *Nature* 438:144–46
Morgan JK, Moore GF, Clague DA. 2003. Slope failure and volcanic spreading along the submarine south flank of Kilauea volcano, Hawaii. *J. Geophys. Res.* 108(B9):2415
Morgan JK, Silver E, Camerlenghi A, Dugan B, Kirby S, et al. 2009. Addressing geohazards through ocean drilling. *Sci. Drill.* 7:15–30
Nooner SL, Eiken O, Hermanrud C, Sasagawa GS, Stenvold T, Zumberge MA. 2007. Constraints on the in situ density of CO_2 within the Utsira formation from time-lapse seafloor gravity measurements. *Int. J. Greenh. Gas Control* 1:198–214
Ohta Y, Hino R, Inazu D, Ohzono M, Ito Y, et al. 2012. Geodetic constraints on afterslip characteristics following the March 9, 2011, Sanriku-oki earthquake, Japan. *Geophys. Res. Lett.* 39:L16304
Owen SE, Bürgmann R. 2006. An increment of volcano collapse: kinematics of the 1975 Kalapana, Hawaii, earthquake. *J. Volcanol. Geotherm. Res.* 150:163–85
Ozawa S, Nishimura T, Suito H, Kobayashi T, Tobita M, Imakiire T. 2011. Coseismic and postseismic slip of the 2011 magnitude-9 Tohoku-oki earthquake. *Nature* 475:373–76
Phillips KA, Chadwell CD, Hildebrand JA. 2008. Vertical deformation measurements on the submerged south flank of Kilauea volcano, Hawai'i reveal seafloor motion associated with volcanic collapse. *J. Geophys. Res.* 113:B05106
Polster A, Fabian M, Villinger H. 2009. Effective resolution and drift of Paroscientific pressure sensors derived from long-term seafloor measurements. *Geochem. Geophys. Geosyst.* 10:Q08008
Sasagawa G, Zumberge MA. 2013. A self-calibrating pressure recorder for detecting seafloor height change. *IEEE J. Ocean. Eng.* 38:447–54
Satake K, Tanioka Y. 1999. Sources of tsunami and tsunamigenic earthquakes in subduction zones. *Pure Appl. Geophys.* 154:467–83
Sato M, Fujita M, Matsumoto Y, Ishikawa T, Saito H, et al. 2013. Interplate coupling off northeastern Japan before the 2011 Tohoku-oki earthquake, inferred from seafloor geodetic data. *J. Geophys. Res. Solid Earth* 118:3860–69
Sato M, Ishikawa T, Ujihara N, Yoshida S, Fujita M, et al. 2011a. Displacement above the hypocenter of the 2011 Tohoku-oki earthquake. *Science* 332:1395
Sato M, Saito H, Ishikawa T, Matsumoto Y, Fujita M, et al. 2011b. Restoration of interplate locking after the 2005 Off–Miyagi Prefecture earthquake, detected by GPS/acoustic seafloor geodetic observation. *Geophys. Res. Lett.* 38:L01312
Scholz CH. 1998. Earthquakes and friction laws. *Nature* 391:37–42
Schwartz SY, Rokosky JM. 2007. Slow slip events and seismic tremor at circum-Pacific subduction zones. *Rev. Geophys.* 45:RG3004
Smith WHF, Sandwell DT. 1997. Global seafloor topography from satellite altimetry and ship depth soundings. *Science* 277:1957–62
Spiess FN. 1980. Acoustic techniques for marine geodesy. *Mar. Geod.* 4:13–27
Spiess FN. 1985. Suboceanic geodetic measurements. *IEEE Trans. Geosci. Remote Sens.* GE-23:502–10
Spiess FN, Chadwell CD, Hildebrand JA, Young LE, Purcell JGH, Dragert H. 1998. Precise GPS/acoustic positioning of seafloor reference points for tectonic studies. *Phys. Earth Planet. Inter.* 108:101–12
Spiess FN, Cox CS, Hays EE, Porter RP, Roberts FA. 1983. *Seafloor Referenced Positioning: Needs and Opportunities.* Washington, DC: Natl. Acad. Press
Spiess FN, Loughridge MS, McGehee MS, Boegeman DE. 1966. An acoustic transponder system. *Navigation* 13:154–61
Sweeney AD, Chadwell CD, Hildebrand JA, Spiess FN. 2005. Centimeter-level positioning of seafloor acoustic transponders from a deeply-towed interrogator. *Mar. Geod.* 28:39–70
Tolstoy M, Constable S, Orcutt J, Staudigel H, Wyatt FK, Anderson G. 1998. Short and long baseline tiltmeter measurements on Axial Seamount, Juan de Fuca Ridge. *Phys. Earth Planet. Inter.* 108:129–41
Uchida N, Matsuzawa T. 2013. Pre- and postseismic slow slip surrounding the 2011 Tohoku-oki earthquake rupture. *Earth Planet. Sci. Lett.* 374:81–91
Wang L, Shum CK, Simons FJ, Tapley B, Dai C. 2012. Coseismic and postseismic deformation of the 2011 Tohoku-oki earthquake constrained by GRACE gravimetry. *Geophys. Res. Lett.* 39:L07301

Wessel P, Smith WHF. 1998. New, improved version of Generic Mapping Tools released. *Eos Trans. AGU* 79:579

Wills PB, Hatchell PJ, Bourne SJ. 2008. Time-lapse measurements of shallow horizontal wave velocity over a compacting field. *EAGE Expand. Abstr.* 70:G039

Wilson DS. 1993. Confidence intervals for motions and deformation of the Juan de Fuca plate. *J. Geophys. Res.* 98(B9):16053–71

Zumberge M. 1997. Precise optical path length measurement through an optical fiber: application to seafloor strain monitoring. *Ocean Eng.* 24:532–42

Zumberge M, Alnes H, Eiken O, Sasagawa G, Stenvold T. 2008. Precision of seafloor gravity and pressure measurements for reservoir monitoring. *Geophysics* 73:WA133–41

Annual Review
of Earth and
Planetary Sciences
Volume 42, 2014

Contents

Indexes

Errata

An online log of corrections to *Annual Review of Earth and Planetary Sciences* articles may be found at http://www.annualreviews.org/errata/earth